Available online at www.sciencedirect.com
SCIENCE DIRECT®
International Journal of Mass Spectrometry 229 (2003) 35–45
International Journal of Mass Spectrometry
www.elsevier.com/locate/ijms

FRET measurements of trapped oligonucleotide duplexes

Allison S. Danell, Joel H. Parks*

The Rowland Institute at Harvard, 100 Edwin H. Land Boulevard, Cambridge, MA 02142, USA

Received 8 January 2003; accepted 25 February 2003

Abstract

Sensitive methods developed to measure laser-induced fluorescence from trapped ions have been applied to study the intermediate states of the dissociation of oligonucleotide duplexes. Double-stranded oligonucleotide anions were prepared with FRET donor/acceptor pairs attached. Gas phase ions were generated by electrospray ionization and injected into a heated quadrupole ion trap where they were stored and exposed to Nd:YAG laser pulses at 532 nm. The dissociation of the duplexes into single strands was monitored by both fluorescence and mass spectra. The comparison of the degree of dissociation of the duplex observed in the mass spectra to the fluorescence intensity of the donor allows for the determination of the intermediate conformations of the unzipping duplex. The observation of changes in the donor fluorescence in the absence of single strands correlates with an intermediate state characterized by threshold unzipping at the weaker binding end of the duplex. These data are consistent with a model of intermediate state formation as a function of temperature. These studies suggest that FRET methods will be useful to obtain direct measurements, which characterize the dynamics of conformational changes of biomolecules in the gas phase.

Keywords: FRET; Oligonucleotides; Biopolymers

1. Introduction

There is a growing body of research [1,2] that has focused on measuring the dynamics and structure of biopolymers in a gas phase environment. The ability to isolate and study molecular processes in gas phase avoids the complexity accompanying solution phase measurements, which is clearly an advantage for the interpretation of microscopic details. Furthermore, such studies offer the possibility that an understanding of gas phase dynamics, and the variations introduced by hydration of the biomolecule, will lead to a correlation with solution phase measurements. This paper introduces biopolymer fluorescence techniques which offer the possibility to directly observe conformational dynamics in gas phase.

Recently developed fluorescence techniques [3] have been applied to measure fluorescence resonance energy transfer (FRET) [4] in trapped biopolymer ions. Quadrupole ion traps provide a controlled environment in which fluorescence measurements can be performed on an ensemble of ions over timescales sufficient to consider small ion numbers and slow reaction rates. It will be demonstrated that this fluorescence technique can be used to detect conformational changes of gas phase species. The extension of FRET methods, widely used in solution studies, to measurements of trapped biopolymer ions provides the opportunity to *directly* correlate changes in fluorescence intensity with changes in the average conformation of biopolymer molecules. This paper describes the application of FRET methods to investigate the gas phase dissociation dynamics of double strand oligonucleotide anions [5]. The trap offers a unique capability to correlate in situ fluorescence data with ion mass spectra leading to a new approach to study the intermediate states immediately preceding dissociation of the double-stranded oligonucleotide ions.

Section 2 describes the experimental methods to prepare oligonucleotides derivatized with appropriate fluorophores and the apparatus to obtain fluorescence and mass spectra data. Section 3 presents initial measurements [6,7] of trapped 14-mer double-stranded oligonucleotides which display characteristics consistent with a metastable intermediate state associated with the dissociation dynamics into single strands.

* Corresponding author. Tel.: +1-617-497-4653; fax: +1-617-497-4627.
E-mail address: parks@rowland.harvard.edu (J.H. Parks).

1387-3806/$ – see front matter © 2003 Elsevier B.V. All rights reserved.
doi:10.1016/S1387-3806(03)00253-7

2. Experimental

2.1. Oligonucleotide FRET preparation

Oligonucleotides were derivatized with amino groups at either the 3′ or 5′ end of the strand, and were conjugated with fluorophores that have *N*-succinimydil ester groups that react with the amino functionalities. The fluorophores, analogs of tetramethylrhodamine (TMR) and texas red (TR), are from the BODIPY line of products available from Molecular Probes. The chemical structure for these fluorophores are shown in Fig. 1a and b and the published [8] absorption and emission spectra measured in solution are shown in Fig. 1c. Although these dyes were designed to be charge–neutral in solution, the dye absorption and emission spectra cannot be assumed to be identical in gas phase. To identify the extent to which environment polarity affects the dye spectra, measurement of the absorption and emission of both BODIPY-TMR and BODIPY-TR dyes were compared for different solvents using a Spex Fluorolog spectrometer. The measured spectra for BODIPY-TMR in methanol and hexane, shown in Fig. 2a, and for BODIPY-TR in methanol and pentane, shown in Fig. 2b, were found to be very similar so that we assume the gas phase and solution spectra will not be significantly different. Since these dyes will be used at elevated temperatures, the possibility that the relative quantum yield varies with temperature was also investigated. Both BODIPY-TMR and BODIPY-TR fluorescence was measured at 23 and 60 °C was found not to vary significantly for either dye, as shown in Fig. 3.

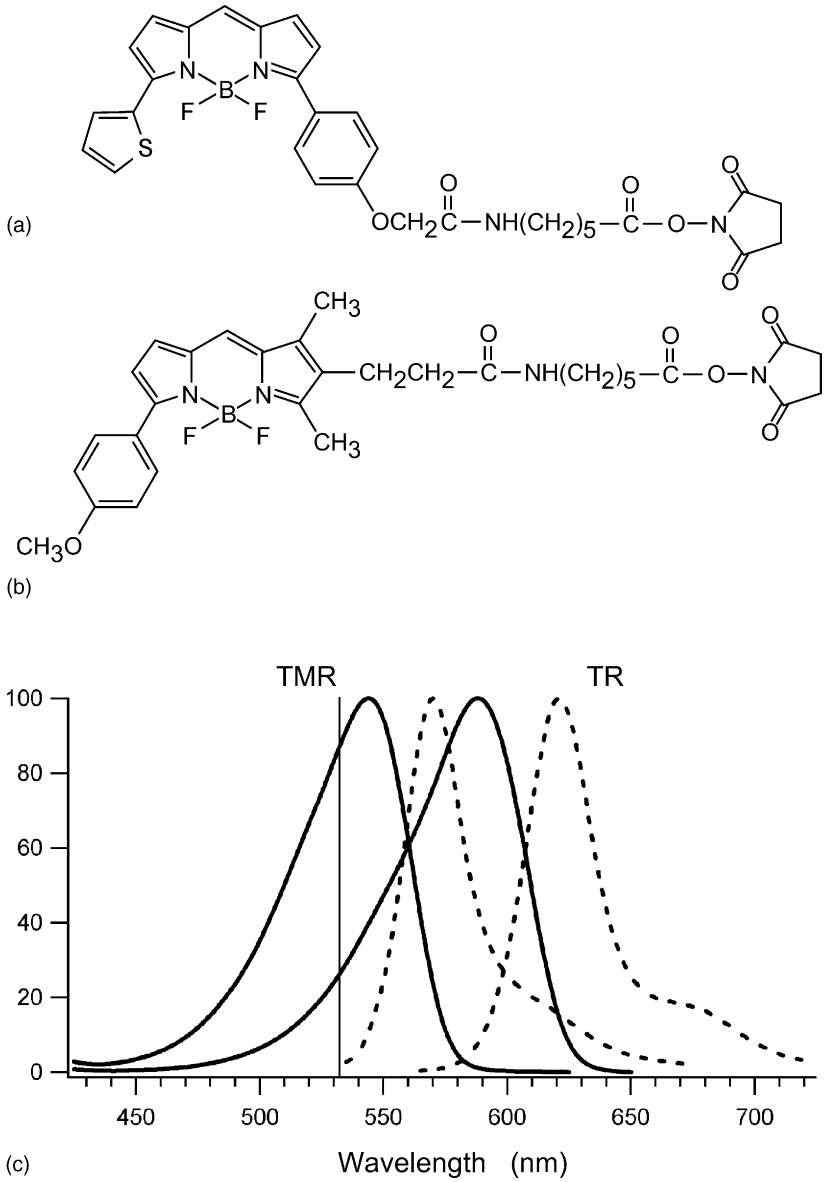

Fig. 1. Structures of (a) BODIPY® TR-X, SE; (b) BODIPY® TMR-X, SE and their absorption (solid curve) and emission (dashed curve) spectra. The laser wavelength (532 nm) is indicated by the vertical line.

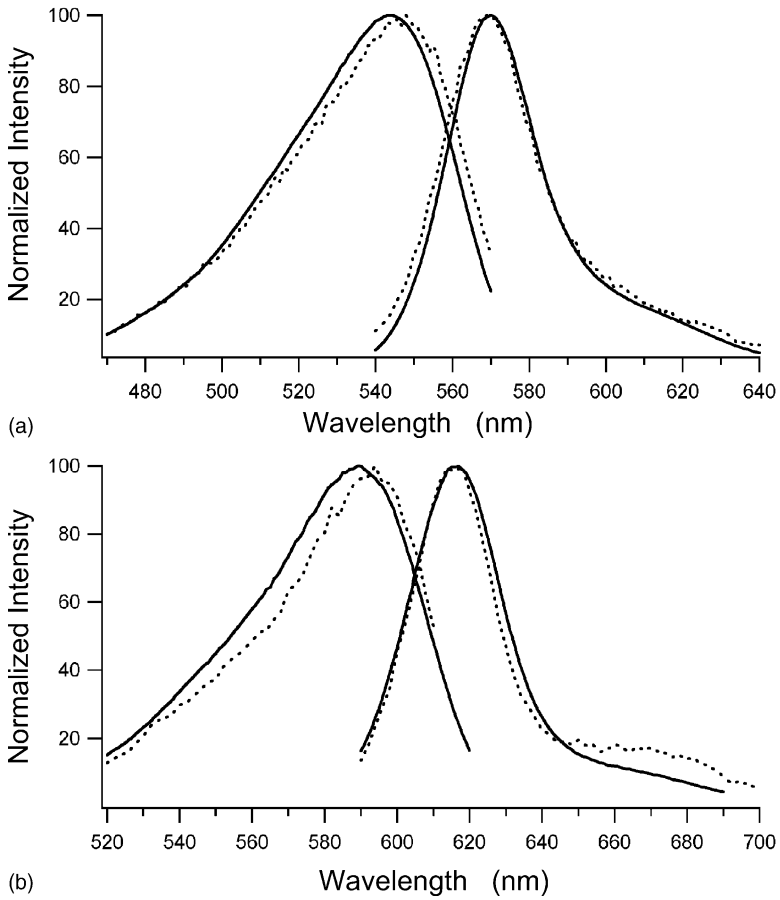

Fig. 2. Absorption and emission spectra of (a) BODIPY® TMR in methanol (solid curve) and hexane (dashed curve) solvents at $T = 20\,^{\circ}C$ and (b) BODIPY® TR in methanol (solid curve) and pentane (dashed curve) solvents at $T = 20\,^{\circ}C$.

Oligonucleotides were obtained commercially (Synthegen Modified Oligonucleotides, Houston, TX). Dye conjugation has been performed in-house following the Molecular Probes protocol, but final products also have been obtained commercially (Synthegen Modified Oligonucleotides). Complementary single strands were combined at a concentration of 50 μM in a 50 mM ammonium acetate solution and annealed for 8 m at ∼90 °C, then slowly cooled to room temperature over 2–3 h to form the oligonucleotide duplexes. The presence of duplexes was verified in solution by absorption spectroscopy. The absorbance at 260 nm versus temperature profile is shown in Fig. 4 for the following 14-mer model sequence:

BODIPY-TMR-5′-AATTAATCCGGCCG-3′

BODIPY-TR-3′-TTAATTAGGCCGGC-5′

Because the single-stranded oligonucleotides have higher extinction coefficients than the double-stranded oligonucleotide, UV spectrophotometry can be used to confirm the presence of the 14-mer duplex in solution. The thermal denaturation curve of the 14-mer duplex measured by UV absorbance displayed in Fig. 4 provides a unique signature for the presence of the duplex species. Final concentrations for nanoelectrospray ionization (nanoESI) solutions were 5–10 μM in 50:50 methanol/water or 60:20:20 acetonitrile/isopropyl alcohol/water with the final ammonium acetate concentration between 5 and 10 mM.

2.2. Fluorescence detection and mass spectra

Details of the quadrupole ion trap/laser-induced fluorescence instrument shown in Fig. 5 have been given elsewhere [3]. Ions generated by nanoESI enter an octapole ion guide from which they are injected into a quadrupole ion trap. The trap electrodes and He gas inlet reservoir are seated in a copper housing which is heated by heater cartridges to a maximum temperature of 170 °C (Model 965 temperature controller, Watlow) with a temperature precision of ±1 °C. The He bath gas pressure was ∼0.4 mTorr and was pulsed to ∼1 mTorr before loading ions into the ion trap. Under these conditions, the trapped ions were equilibrated by $>10^5$ collisions with the He bath gas which was maintained at the temperature of the trap electrodes. These ions are exposed to Nd:YAG laser pulses (∼15 ns, 100 Hz) at the frequency doubled wavelength 532 nm. The laser beam diameter has been reduced to ∼150 μm to eliminate scattering on trap apertures and electrodes. The resulting laser–ion interaction

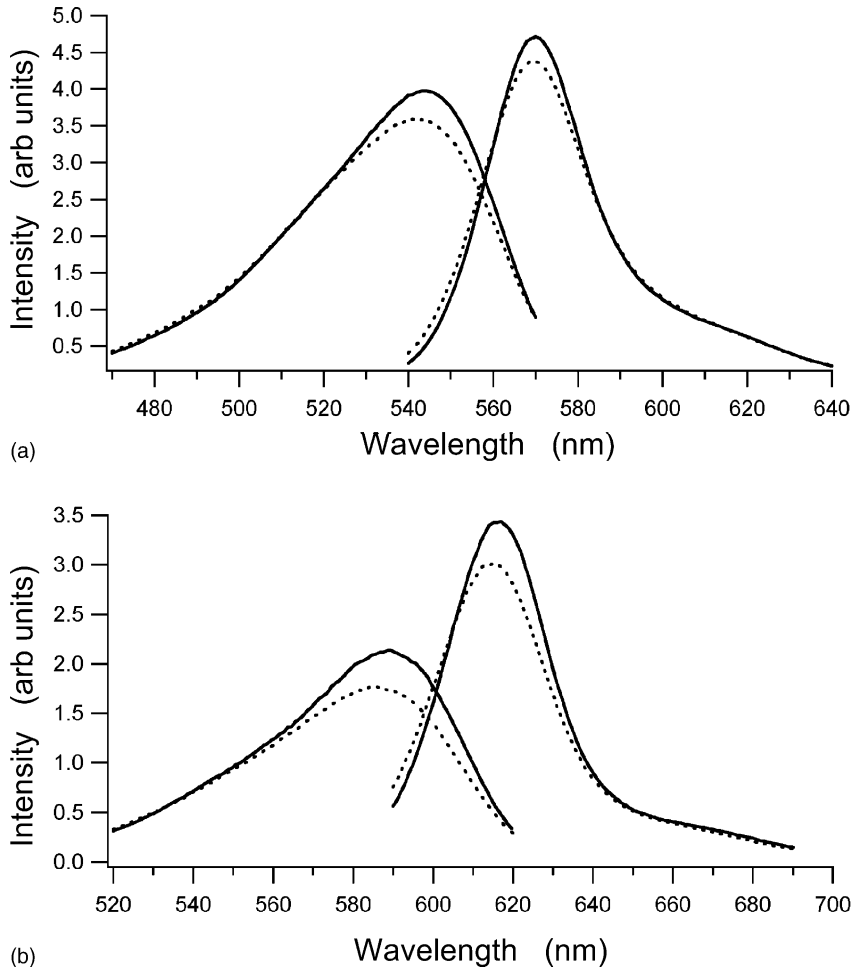

Fig. 3. Absorption and emission spectra of (a) BODIPY® TMR at $T = 20\,^{\circ}C$ (solid curve) and $T = 59\,^{\circ}C$ (dashed curve) in methanol solvent; (b) BODIPY® TR in methanol solvent at $T = 20\,^{\circ}C$ (solid curve) and $T = 59\,^{\circ}C$ (dashed curve).

is limited to a volume of $\sim 10^{-5}\,cm^3$ which is ~0.03–0.15 of the total ion cloud volume, depending on trap operating parameters and temperature. The bandpass filter used for these experiments passes wavelengths 535–580 nm, corresponding to the donor fluorescence bandwidth (see Fig. 1c).

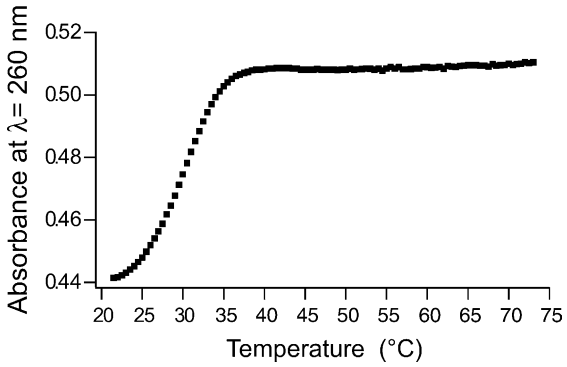

Fig. 4. Absorption at 260 nm vs. temperature for solution of BODIPY-TMR-5′-AATTAATCCGGCCG-3′ and 5′-CGGCCGGATTAATT-3′-BODIPY-TR.

In these experiments, only the donor fluorescence was detected. The fluorescence was focused through an aperture of ≤1 mm positioned before a photomultiplier detector (PMT; Hamamatsu R1463). This limited the fluorescence collection to a solid angle defined by the laser–ion interaction volume which helped to minimize the detection of background laser scattering. The most significant achievement in the development of these methods for measuring laser-induced fluorescence from trapped ions has been the elimination of background laser scattering *during* the excitation pulse.

An important advantage provided by the ion trap is the ability to compare the fluorescence and the associated mass spectra of the trapped ions. Examples of the detected mass and fluorescence spectra for 4- charge state ions of AAAAGCAAAA derivatized with BODIPY-TMR at its 3′ end ($[5'$-AAAAGCAAAA-$3'$-BODIPY-TMR$]^{4-}$) are shown in Fig. 6a and b. The peak area for the 4- charge state ions shown in Fig. 6a corresponds to the detection of approximately 3650 ions by the Channeltron electron multiplier. Thus, approximately 7300 ions were present in the trap during the 60 s of laser irradiation. An estimated ~350

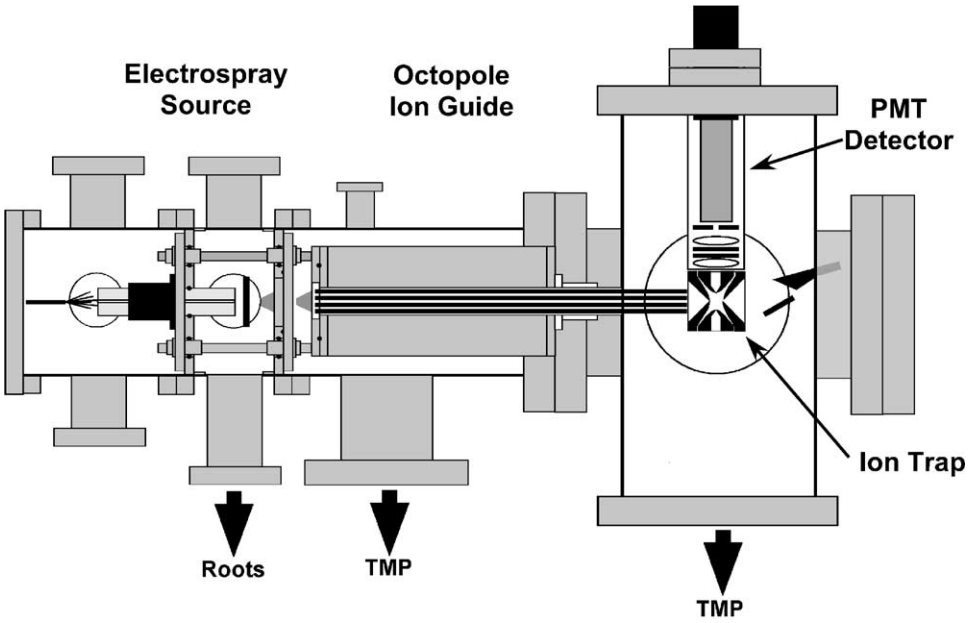

Fig. 5. Schematic of the ESI/ion trap/laser-induced fluorescence assembly showing the spray, heated capillary, shutter, two skimmers, 30 cm octapole ion guide leading into the quadrupole ion trap and finally the ion detector. Shown above the trap is the (*xyz*) translatable fluorescence detection apparatus including two lenses, filters, 1 mm aperture and PMT.

ions were irradiated by the laser beam, based on ion cloud density calculations and the volume of overlap between the ion cloud and the laser beam. Fig. 6b shows the pulsed fluorescence signals corresponding to the photoelectrons detected during each 15 ns laser pulse. Fig. 6c demonstrates the low background signal achieved in the absence of stored ions. This 10-mer oligonucleotide sequence and several other sequences of 7–14 bases in length have been successfully analyzed with mass spectrometry and fluorescence in the gas phase. This demonstration of laser-induced fluorescence of derivatized biomolecules in the gas phase is the first known example of its kind.

The fluorescence intensity emitted by trapped ions increased nonlinearly with increasing ion number, as shown for [BODIPY-TMR-5′-AATTAATCCGGCCG-3′]$^{6-}$ in Fig. 7. This behavior has been observed previously for singly charged ions [3] and was attributed to a space charge-limited ion cloud density that approached a constant value as a result of increasing electrostatic repulsion [9]. The ability to estimate the effects of space charge on fluorescence intensity is important for biopolymer ions because these multiply charged ions result in saturation of the ion density at relatively small ion numbers (∼1000 ions). The number of ions in the overlap volume of the laser and ion-cloud was estimated by calculating the ion density $n(z, r)$ within a mean field approximation [10,11]. The ion number was then obtained by integrating $n(z, r)$ throughout the overlap volume defined by the laser cross-section. Further details of this calculation, which accurately reproduced the ion number dependence exhibited by the fluorescence data as indicated in Fig. 7, will be presented elsewhere.

3. Duplex dynamics: intermediate states

Previous measurements of duplex dissociation in gas phase [5] relied on mass spectrometry to detect the onset of single strand ions. Measurements of this type preclude the observation of intermediate or transitional states prior to dissociation. The departure from two-state thermodynamics has been observed in solution phase measurements of the melting temperature of oligonucleotide duplexes with less than 20 base pairs [12]. The possibility that such states are present in gas phase dynamics was suggested by collision-induced dissociation of oligonucleotides [13,14]. The capability of applying FRET fluorescence techniques to detect and quantify biopolymer dynamics can be investigated by the study of such intermediate states. The emphasis in the present experiments was to configure a duplex composition that would exhibit an unambiguous dynamic signature of an intermediate state. These initial measurements will help to identify the sensitivity of FRET methods to detect and identify conformational change in gas phase biopolymers.

3.1. Intermediate state model

One of the goals of developing this technology is to be able to monitor conformational changes of noncovalent complexes in the gas phase with FRET. Thus, changes in fluorescence intensity can be correlated with changes in average conformation of the species of interest. To this end, we designed a 14-mer model oligonucleotide duplex with the sequence AATTAATCCGGCCG and its complement.

This oligonucleotide sequence was chosen to strongly bias the possibility that a long-lived intermediate state will

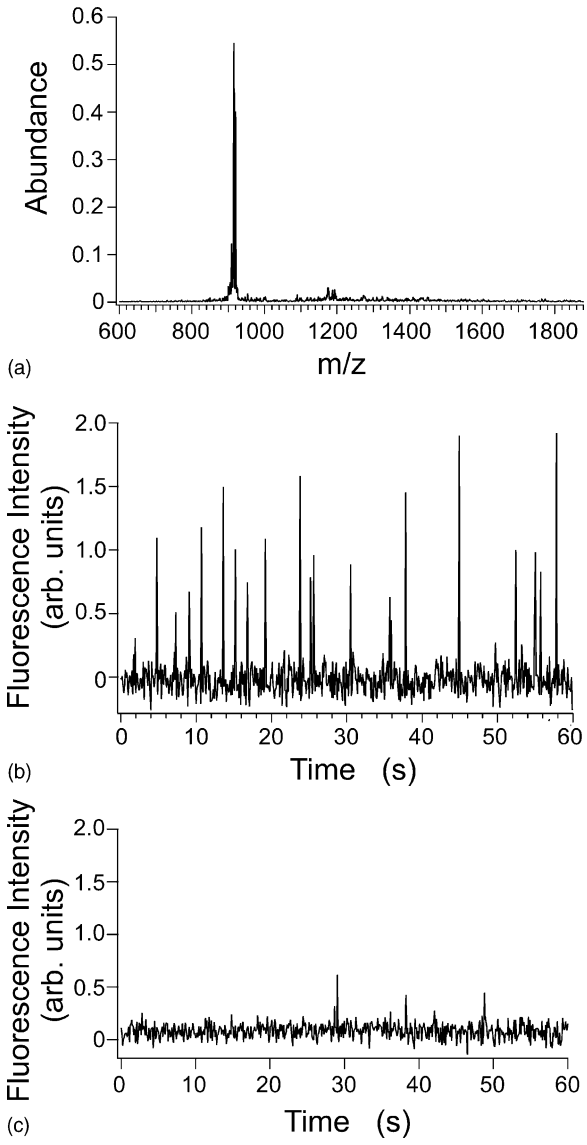

Fig. 6. (a) Single scan mass spectrum of 5′-AAAAGCAAAA-3′-BODIPY-TMR; isolated 4- charge state at $q_z = 0.58$, $T = 25\,^{\circ}\mathrm{C}$. (b) Single scan fluorescence spectrum from [5′-AAAAGCAAAA-3′-BODIPY-TMR]$^{4-}$; pulse energy: 0.90 μJ. (c) Representative spectrum of PMT signal with no ions loaded in ion trap.

be present. Solution phase melting experiments have established that terminal bases composed of A·T pairs have a tendency to fray, or break the bonds near the duplex terminal [12]. In addition, the greater stability of C·G bonds relative to those of A·T suggested that a duplex sequence composed of A·T pairs followed by C·G pairs could provide sufficient enthalpy bias to form a long-lived metastable intermediate state. Dissociation of the duplex into single strands, often described as “unzipping”, would more likely start from the end containing the A·T base pairs. Consequently, the members of the FRET pair were placed on the appropriate termini to result in increased distance between the dyes at the beginning of the dissociation process.

A kinetic model based on the simplified potential energy diagram shown in Fig. 8 was formulated to describe the dissociation of the oligonucleotide duplex through an intermediate state. Fig. 8 depicts potential barriers and transition rates between a duplex state (1) and an intermediate state (2) and also between the intermediate state and a dissociative state (3). In this case the intermediate state represents a partially unzipped oligonucleotide. The rate equations and solutions characterizing these transitions are presented in Appendix A. As indicated in Fig. 8, the ability to observe an intermediate state (2) depends on the relative barrier heights E_{12} and E_{23}. If $E_{12} \gg E_{23}$, the dissociative transition will be essentially a two-state process as indicated by the dashed curve. In this case the kinetic rate through the intermediate state (2) will be fast enough that it will not be detected by these fluorescence measurements. However, if $E_{12} \ll E_{23}$, the transition will be slower so that the molecule can reside in the intermediate state long enough to increase the probability of detection by fluorescence.

Solutions of the rate equations were calculated for a model duplex composed of partially complementary 14-mer strands and are plotted in Fig. 9a–d. As discussed in more detail below, a combination of the sequences AATTAAT and CCGGCCG was chosen in order to take advantage of previous measurements [5] of gas phase dissociation rates for duplexes composed of these sub-sequences. As a result, this model includes rates which are realistic estimates for the various transitions of the experimental duplex. Specifically, the dissociation rates for d(AATTAAT)$_2{}^{3-}$ and d(CCGGCCG)$_2{}^{3-}$ were previously measured as $k_{\mathrm{A{\cdot}T}} = 10^{15.5}\exp(-1.44/kT)$ (s^{-1}) and $k_{\mathrm{C{\cdot}G}} \leq 10^{16.5}\exp(-1.65/kT)$ (s^{-1}) where the activation energies are in units of eV and the duplex is assumed to be equilibrated at temperature T. In the rate equations describing the kinetics, the rates identified in Fig. 8 are approximated by taking $k_{12} \approx k_{\mathrm{A{\cdot}T}}$ and $k_{23} \approx k_{\mathrm{C{\cdot}G}}$. The reverse rate k_{21} was estimated by taking $k_{12}/k_{21} = \exp(\Delta G_{12}/kT)$ where the free energy change, ΔG_{12}, was calculated from [12].

The model yields the total fluorescence emitted by the ensemble of oligonucleotides distributed over the three states by the temperature-dependent kinetics. The donor fluorophore is within 3–5 Å of the acceptor in state 1 so that the donor fluorescence is negligible. The dissociated donor strand has maximum fluorescence in state 3, and the fluorescence intensity in the intermediate state 2 depends strongly on the average acceptor–donor separation, $\langle R_2 \rangle$, relative to the Förster distance, R_0. At this distance, the energy transfer rate reduces the donor fluorescence by approximately a factor of 2. The graphs display both the donor fluorescence intensity and the single strand density for different values of $\langle R_2 \rangle / R_0$. In Fig. 9a, $\langle R_2 \rangle / R_0 = 0.65$ is sufficiently small that the FRET donor fluorescence is significant only for temperatures for which the duplex dissociates. As $\langle R_2 \rangle / R_0$ increases, Fig. 9b–d, the fluorescence intensity is observed to increase at temperatures for which dissociation into single strands does not occur: the experimental signature of

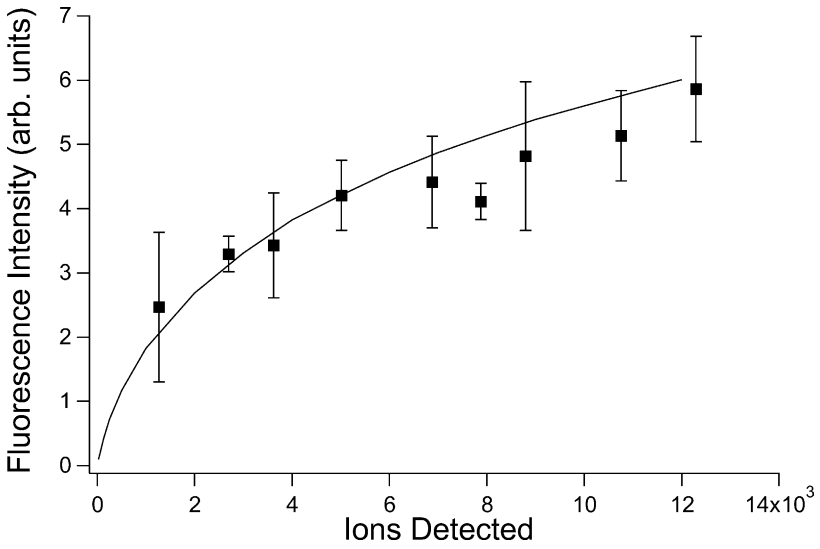

Fig. 7. Fluorescence intensity from [BODIPY-TMR-5′-AATTAATCCGGCCG-3′]$^{6-}$ as a function of number of ions detected; pulse energy: 1.0 μJ; isolated 6- charge state at $q_z = 0.54$, $T = 25\,^{\circ}C$. Solid curve derived from space charge calculations of the ion densities.

the intermediate state. For $\langle R_2 \rangle / R_0 \geq 1$, the donor fluorescence increases rapidly with temperature and significantly distorts the sigmoid shape of the temperature dependence. Comparing FRET fluorescence data with such an intermediate state model will help to identify the presence of such an intermediate state and the degree to which this simple kinetic model characterizes such transitions.

3.2. FRET measurements of model 14-mer duplex

Duplex ions were identified in the gas phase by the nanoESI mass spectrum of a 10 μM solution containing the complementary 14-mer model sequences as shown in Fig. 10. Double-stranded oligonucleotide ions were unambiguously identified only at the odd charge states in the mass spectrum. The 7- charge state ions of the duplex were isolated in the quadrupole ion trap and fluorescence data were acquired for 60 s periods at emission wavelengths corresponding to fluorescence from the donor molecule. An example of the data obtained under these conditions is shown in Fig. 11. The mass spectrum in Fig. 11a shows that no product ions were formed when the duplex ions were held at 117 °C for 60 s. Fig. 11b shows weak fluorescence from the donor molecule during the same time period. At room temperature, no donor fluorescence was expected because FRET should be occurring at an efficient rate. A relatively small amount of fluorescence was detected by the PMT at room temperature, which could be due to leakage of acceptor fluorescence or incomplete energy transfer from donor to acceptor. The room temperature donor fluorescence from the duplex was considered to be the baseline for subsequent measurements.

The temperature range over which mass and fluorescence spectra were acquired was set below the threshold

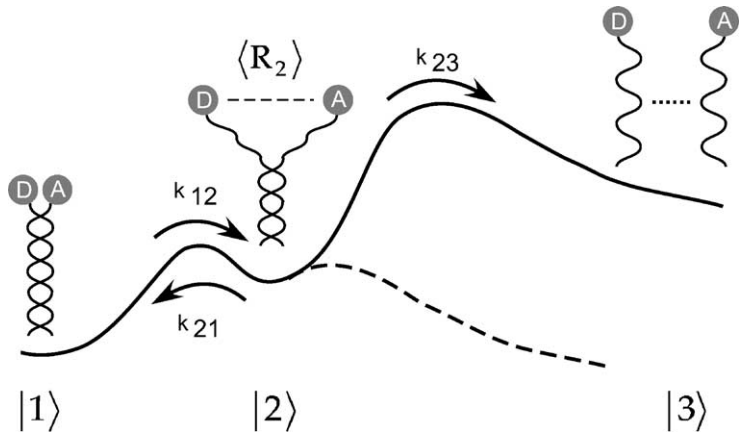

Fig. 8. Simplified potential energy diagram indicating the kinetics associated with the melting transition of a duplex to single strands which includes a metastable intermediate state. The dashed curve represents a potential energy which would characterize a “two-state” transition. The duplex is shown with donor (D) and acceptor (A) fluorophores attached. The intermediate state is characterized by the partially “unzipped” duplex.

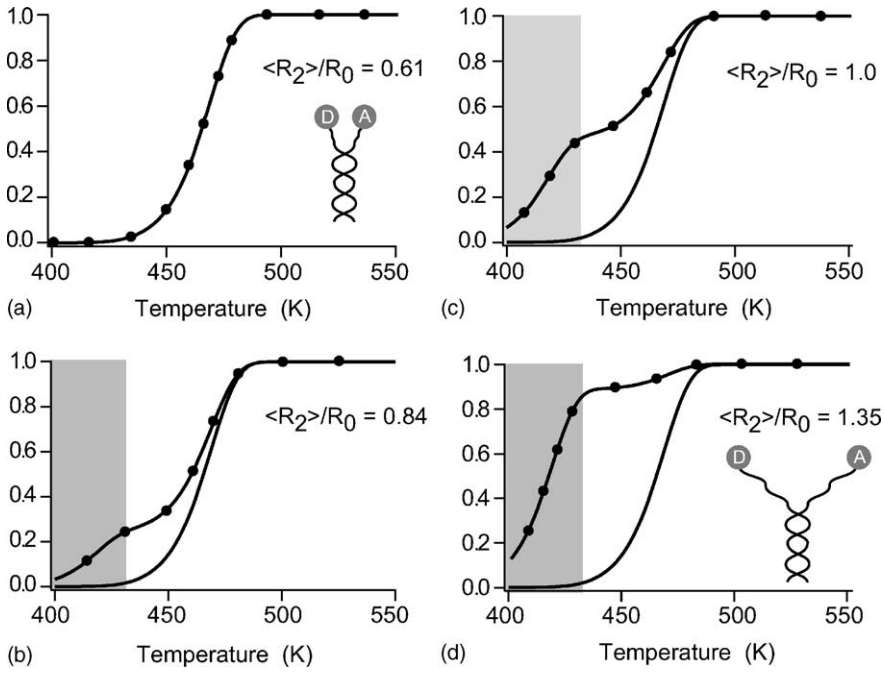

Fig. 9. Plots of the rate equation solutions calculated for the rates given in Section 3.1 showing the population of the metastable state (●) and the dissociative state (solid curve) vs. temperature for different values of the parameter $\langle R \rangle / R_0$ (a–d). The shaded portion of each plot indicates the temperature range over which there is negligible dissociation of the duplex.

temperature of ∼130 °C at which the duplex ions were observed to fragment during the 60 s storage interval. The absence of product ions was verified in the mass spectrum that was acquired after each 60 s fluorescence measurement, confirming that fluorescence measurements were made of intact duplex ions.

The data acquisition illustrated in Fig. 11 was conducted at several different temperatures, and the resulting fluorescence intensities are shown in Fig. 12a. The fluorescence intensities from the 14-mer *single* strand derivatized with the donor are also shown in Fig. 12b. The increase in fluorescence in Fig. 12a can be attributed to increased distance between the FRET donor and acceptor fluorophores. The increased separation between the FRET pair was not a result of dissociation of the duplex into single strands, because single-stranded ions were not observed in the mass spectrum. Note that in Fig. 12b, there is no pattern of increased fluorescence over this temperature range from a single strand derivatized with the FRET donor fluorophore. The detection of a slight increase in donor fluorescence from the duplex ions suggests that the duplex ions were undergoing a conformational change occurring before complete dissociation into single strands.

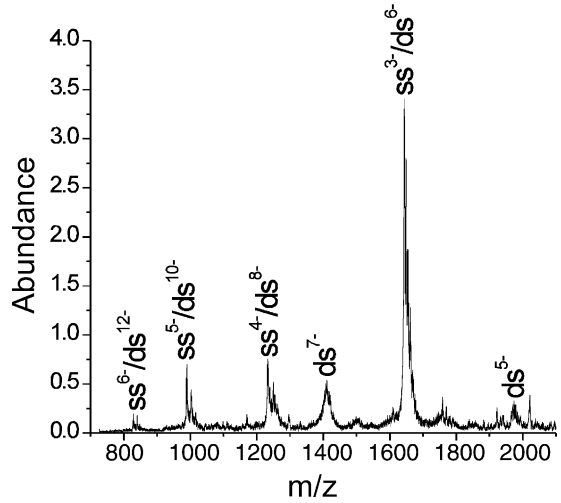

Fig. 10. Mass spectrum of the 14-mer duplex of BODIPY-TMR-5′-AATTAATCCGGCCG-3′ and 5′-CGGCCGGATTAATT-3′-BODIPY-TR; single strands denoted with ss, double strands with ds.

3.3. Data–model comparison

The FRET data has been compared with calculations described in Appendix A which are based on the intermediate state model described in Section 3.1. The FRET data obtained for the complementary 14-mer duplex

BODIPY-TMR-5′-AATTAATCCGGCCG-3′

BODIPY-TR-3′-TTAATTAGGCCGGC-5′

will be compared with a calculation performed, as described above, with rates derived from similar but only partially complementary strands

BODIPY-TMR-5′-AATTAATCCGGCCG-3′

BODIPY-TR-3′-TAATTAAGCCGGCC-5′

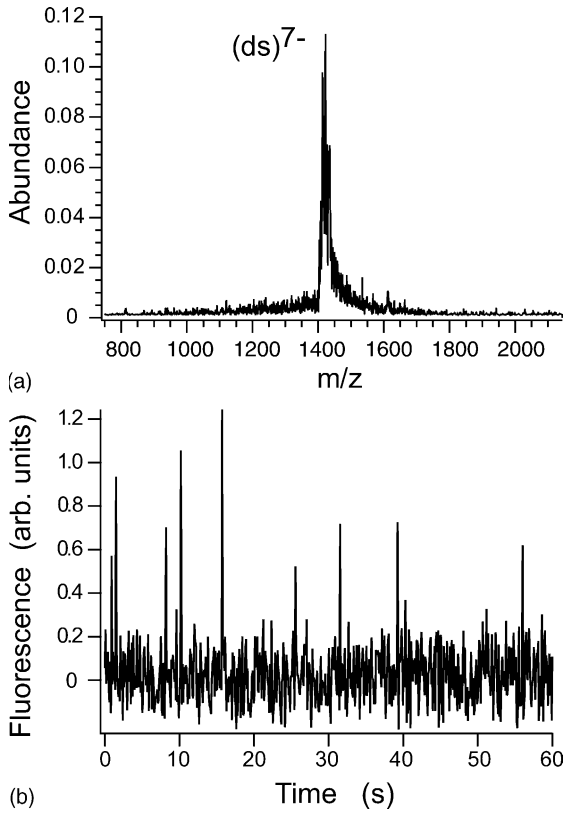

Fig. 11. (a) Single scan mass spectrum of solution of BODIPY-TMR-5′-AATTAATCCGGCCG-3′ and 5′-CGGCCGGATTAATT-3′-BODIPY-TR; isolated 7- charge state of duplex at $q_z = 0.54$, $T = 117\,^{\circ}\mathrm{C}$. (b) Single scan donor fluorescence spectrum from 7- ion of duplex of BODIPY-TMR-5′-AATTAATCCGGCCG-3′ and 5′-CGGCCGGATTAATT-3′-BODIPY-TR; pulse energy: 1.0 μJ.

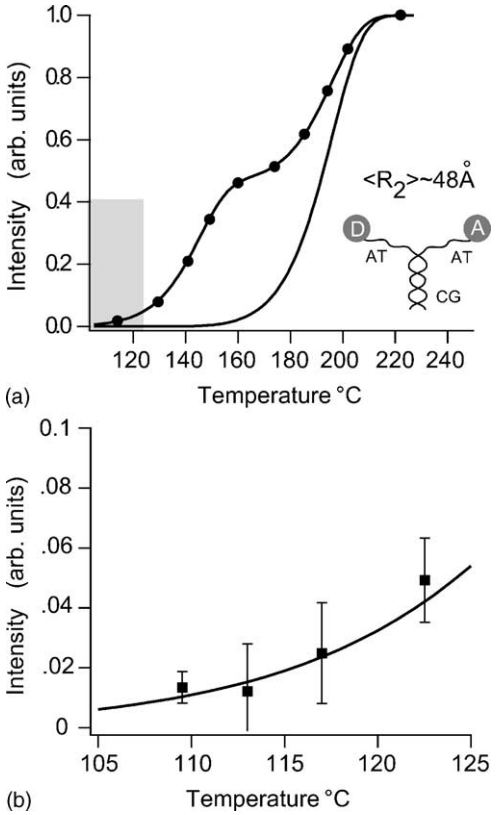

Fig. 13. (a) Plot of the rate equation solutions calculated for the rates given in Section 3.1 showing the population of the metastable state (●) and the dissociative state (solid curve) vs. temperature for $\langle R_2 \rangle \sim R_0 \sim 48\,\text{Å}$. The shaded portion indicates the temperature range over which data was obtained. (b) Plot of the duplex donor fluorescence intensity data from 7- ion of duplex of BODIPY-TMR-5′-AATTAATCCGGCCG-3′ and 5′-CGGCCGGATTAATT-3′-BODIPY-TR (■) shown in Fig. 12a and the rate equation solution (solid curve) for the metastable state shown in (a).

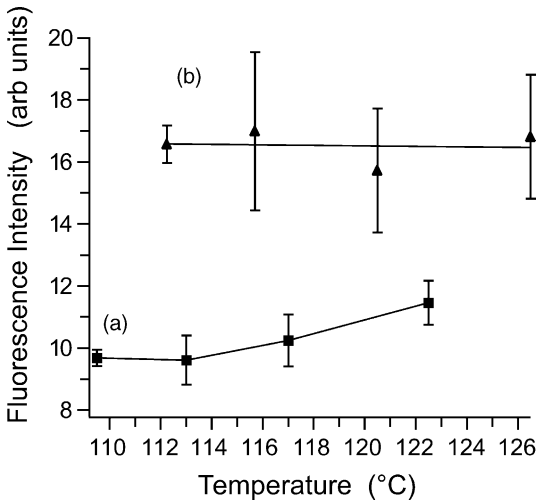

Fig. 12. (a) Donor fluorescence intensities (■) from 7- ion of duplex of BODIPY-TMR-5′-AATTAATCCGGCCG-3′ and 5′-CGGCCG-GATTAATT-3′-BODIPY-TR as a function of temperature; conditions as in Fig. 11. (b) Fluorescence intensities (▲) from 6- ion of single strand BODIPY-TMR-5′-AATTAATCCGGCCG-3′ as a function of temperature.

Consequently, such a comparison will not be reliable for quantitative conclusions regarding the threshold temperature range, but can serve to qualitatively consider the exponential shape of the threshold. To compare FRET data with the intermediate state model requires assumptions of the average fluorophore separation in the transition state. This separation depends on the length of the A·T portion of the oligonucleotide sequence. For the experimental sequence, the length of the 7 bp A·T portion was approximately ∼24 Å and the ensemble average of the fluorophore separation was assumed to occur at ∼180°, a distance of ∼48 Å.

Fig. 13a displays the calculated total fluorescence of the oligonucleotide distribution over the available states as a function of temperature for $\langle R_2 \rangle = 48\,\text{Å}$. The shaded area indicates the temperature range covered by the experimental data. Fig. 13b compares the experimental fluorescence data with the calculation in this temperature range. The data were normalized to the calculated curve at one point but no curve fitting was applied.

This comparison supports the presence and observation of a conformational state in which only a part of the duplex has

become "unzipped". This can be concluded from the fluorescence threshold data in the absence of dissociated single strands which the model predicts for sufficiently small temperatures. The mass spectra show that the double-stranded oligonucleotide remains intact, but the increase in fluorescence of the duplex indicates an increased spatial separation of the dyes conjugated to the oligonucleotides on the A·T ends. This information supports our hypothesis that the 14-mer should separate from the A·T end, and provides us with an estimate of the temperature range over which the dissociation of the 14-mer duplex into single strands should occur.

Furthermore, the shape of the temperature dependence observed in the data was consistent with an exponential growth characterizing the buildup of intermediate state population implied by the model. However, the temperature range covered by the data is not large enough to allow more detailed conclusions. The temperature was constrained to this relatively small interval for two reasons. Up to ∼120 °C, the mass spectrum is unchanged and indicates only the isolated 7- duplex but at higher temperatures, the A·T portion began to fragment into several additional *m*/*z* peaks so that the interpretation of mass spectra became more complex. In addition, the photomultiplier heating also becomes an issue at higher temperatures, since it was mounted within the UHV chamber to maximize detection solid angle. As described below, both these constraints are being eliminated by changes in the ongoing experiments.

4. Summary and conclusions

These experiments demonstrate that measurements of the fluorescence of trapped biopolymer ions can be achieved with sufficient sensitivity and dynamic range to observe FRET signatures associated with small changes in conformation of gas phase ions. The threshold measurement of increasing donor fluorescence demonstrates the promise of the combined fluorescence and mass spectrometry techniques. The observation of intermediate state kinetics helps to evaluate the possibilities for extending these measurements to other dynamical processes. Conformational change in DNA hairpins [15,16], and small peptides including the Trp-cage [17,18] and alpha helices [19,20] provide examples of cooperative dynamics which have been studied in solution phase. They provide excellent opportunities to apply the FRET techniques presented here to study conformational changes characteristic of folding transitions in the gas phase. In each of these examples, complementary detection of acceptor fluorescence will be essential for verification and interpretation of results, and a two-channel detection system is being installed to facilitate simultaneous donor and acceptor fluorescence detection.

It is equally necessary to develop techniques that can help to correlate gas phase results with those of solution phase to understand how the various interactions become modified in the presence of water. In principle, a valuable contribution to this understanding can be achieved if gas phase measurements can be performed as a function of the level of hydration. Such measurements can address the effect of water interactions with hydrogen bonds, charge sites and processes leading to local entropy variations. The hydration of electrosprayed gas phase species has been achieved by various methods [21–23] and continues to receive ongoing consideration [24]. Gas phase experiments have investigated the effect of hydration on biopolymer structure and conformation [25–27]. A goal of this research is to extend the biomolecule measurements introduced in this paper to experiments performed as a function of hydration level.

Acknowledgements

This work is supported by The Rowland Institute at Harvard. The authors would like to thank Prof. Evan Williams for helpful discussions, and Dr. Amit Meller and Dr. Chandran Sabanayagam for helping our introduction to oligonucleotide studies.

Appendix A

The rate equations describing the kinetics shown schematically in Fig. 8 are given by

$$\frac{\mathrm{d}}{\mathrm{d}t}n_1 = -k_{12}n_1 + k_{21}n_2 \tag{A.1}$$

$$\frac{\mathrm{d}}{\mathrm{d}t}n_2 = -k_{23}n_2 + k_{12}n_1 - k_{21}n_2 \tag{A.2}$$

$$\frac{\mathrm{d}}{\mathrm{d}t}n_3 = k_{23}n_2 \tag{A.3}$$

where n_1, n_2 and n_3 represent the ensemble population in states characterized by the initial duplex, intermediate partially unzipped duplex and final dissociated duplex, respectively. The forward and reverse rates of the transition between the initial and metastable intermediate states are k_{12} and k_{21} and the final dissociative rate is k_{23}.

The total power radiated in fluorescence from N_1^* excited donor molecules attached to oligonucleotides in state $|1\rangle$ is expressed by

$$P_1 = N_1^* \frac{h\nu}{\tau_\mathrm{f}} \tag{A.4}$$

where $h\nu$ is the average photon energy and τ_f is the excited state lifetime. Similar equations express the emission for donor molecules attached to oligonucleotides in states $|2\rangle$ and $|3\rangle$. The rate of change of donors in the excited state

$$\frac{\mathrm{d}}{\mathrm{d}t}N_1^* = \frac{I_\mathrm{L}\sigma_\mathrm{abs}}{h\nu}(N_1 - N_1^*) - \frac{N_1^*}{\tau_\mathrm{f}} - k_1^\mathrm{FRET}N_1^* \tag{A.5}$$

is determined by the excitation rate at the laser intensity I_L and absorption cross-section σ_abs, the spontaneous emission

rate, and by the energy transfer rate k_1^{FRET} to the acceptor molecule given by

$$k_1^{\mathrm{FRET}} = \frac{1}{\tau_\mathrm{f}} \left(\frac{R_0}{R_1} \right)^6 \tag{A.6}$$

The energy transfer rate is a rapidly varying function of the ratio of the Förster radius R_0 and the donor–acceptor separation R_1 for an oligonucleotide in state $|1\rangle$. In each state the donor–acceptor separation R_i will be assumed to experience thermal fluctuations described by a normal distribution [28] about an average value $\langle R_i \rangle$ with a standard deviation σ_i. The average steady state excited donor molecules in state $|1\rangle$ is then given by

$$\langle N_1^* \rangle = \int_0^\infty \frac{1}{\sigma_i \sqrt{2\pi}} \frac{\mathrm{d}R_i}{A + (R_0/R_i)^6} \, \mathrm{e}^{-(R_i - \langle R_i \rangle)^2 / 2\sigma_i^2} \tag{A.7}$$

where $A = 1 + \tau_\mathrm{f}(I_\mathrm{L}\sigma_\mathrm{abs}/h\nu)$.

The number of donor molecules are related to the density of oligonucleotides in each dynamic state by $N_i = n_i \delta V$, where δV is the overlap volume of the laser and the ion cloud. Finally, the total average power in fluorescence from donors in all states is

$$\langle P_\mathrm{T} \rangle = \sum_i \langle N_i^* \rangle_{R_i} \frac{h\nu}{\tau_\mathrm{f}} = \delta V I_\mathrm{L} \sigma_\mathrm{abs} \sum_i n_1 \times \int_0^\infty \frac{1}{\sigma_i \sqrt{2\pi}} \frac{\mathrm{d}R_i}{A + (R_0/R_i)^6} \, \mathrm{e}^{-(R_i - \langle R_i \rangle)^2 / 2\sigma_i^2} \tag{A.8}$$

The parameters used in the calculations presented in Section 3 are $I_\mathrm{L} \sim 0.4\,\mathrm{MW/cm^2}$, $\sigma_\mathrm{abs} \sim 10^{-16}\,\mathrm{cm^2}$, $\tau_\mathrm{f} = 3\,\mathrm{ns}$ and $R_0 \sim 48\,\text{Å}$. The absorption rate, $I_\mathrm{L}\sigma_\mathrm{abs}/h\nu \sim 9\,(\mathrm{ns})^{-1}$ is much less than the spontaneous emission rate $1/\tau_\mathrm{f}$, so that $A \sim 1.3$ above. In this model the temperature dependence of $\langle R_i \rangle$, σ_i is not explicitly accounted for. The distribution parameters in Eq. (A.8) are taken to be constant values in each state: $\langle R_i \rangle = 5\,\text{Å}$, $\sigma_1 \sim 2\,\text{Å}$; $\langle R_2 \rangle = 48\,\text{Å}$, $\sigma_2 \sim 10\,\text{Å}$; and $\langle R_3 \rangle = 500\,\text{Å}$, $\sigma_3 \sim 10\,\text{Å}$. These parameters correspond to a close separation in the initial duplex, a value $\langle R_2 \rangle \approx R_0$ in the metastable state, and an arbitrarily large value for the dissociated state. The standard deviations are chosen somewhat arbitrarily, but the calculations are insensitive to this parameter [28]. Since the temperature dependence of the ion cloud volume is proportional to $T^{-3/2}$, the change in n_i due to temperature is negligible over the data range shown in Figs. 12 and 13.

References

[1] C.S. Hoaglund-Hyzer, A.E. Counterman, D.E. Clemmer, Chem. Rev. 99 (1999) 3037.
[2] M.F. Jarrold, Annu. Rev. Phys. Chem. 51 (2000) 179.
[3] J.T. Khoury, S.E. Rodriguez-Cruz, J.H. Parks, J. Am. Soc. Mass Spectrom. 13 (2002) 696.
[4] P.R. Selvin, Nat. Struct. Biol. 7 (2000) 730.
[5] P.D. Schnier, J.S. Klassen, E.F. Strittmatter, E.R. Williams, J. Am. Chem. Soc. 120 (1998) 9605.
[6] J.H. Parks, EuroConference on Fundamental Studies and Applications: Molecules of Biological Interest in the Gas Phase, Wildbad Kreuth, Germany, 2002.
[7] A.S. Danell, J.T. Khoury, J.H. Parks, American Chemical Society Meeting, Boston, MA, 2002.
[8] http://www.molecularprobes.com, accessed on December 2002.
[9] H.G. Dehmelt, in: D.K. Kleppner, F.T. Pipkin (Eds.), Atomic Physics, vol. 7, Plenum Press, New York, 1981, p. 53.
[10] J.H. Parks, A. Szöke, J. Chem. Phys. 103 (1995) 1422.
[11] S. Guan, A.G. Marshall, J. Am. Soc. Mass Spectrom. 5 (1994) 64.
[12] J. SantaLucia Jr., H.T. Allawi, P.A. Seneviratne, Biochemistry 35 (1996) 3555.
[13] V. Gabelica, E. De Pauw, Int. J. Mass Spectrom. 219 (2002) 151.
[14] V. Gabelica, E. De Pauw, J. Am. Soc. Mass Spectrom. 13 (2002) 91.
[15] M.I. Wallace, L. Ying, S. Balasubramanian, D. Klenerman, J. Phys. Chem. B 104 (2000) 11551.
[16] G. Bonnet, O. Krichevsky, A. Libchaber, Proc. Natl. Acad. Sci. U.S.A. 95 (1998) 8602.
[17] L. Qiu, S.A. Pabit, A.E. Roitberg, S.J. Hagen, J. Am. Chem. Soc. 124 (2002) 12952.
[18] C.D. Snow, B. Zagrovic, V.S. Pande, J. Am. Chem. Soc. 124 (2002) 14548.
[19] S. Marqusee, V.H. Robbins, R.L. Baldwin, Proc. Natl. Acad. Sci. U.S.A. 86 (1989) 5286.
[20] R.R. Hudgins, M.F. Jarrold, J. Am. Chem. Soc. 121 (1999) 3494.
[21] S.-W. Lee, P. Freivogel, T. Schindler, J.L. Beauchamp, J. Am. Chem. Soc. 120 (1998) 11758.
[22] S.E. Rodriguez-Cruz, J.S. Klassen, E.R. Williams, J. Am. Soc. Mass Spectrom. 10 (1999) 958.
[23] D. Zhan, J. Rosell, J.B. Fenn, J. Am. Soc. Mass Spectrom. 9 (1998) 1241.
[24] D. Zhan, J.B. Fenn, Int. J. Mass Spectrom. 219 (2002) 1.
[25] S.E. Rodriguez-Cruz, J.S. Klassen, E.R. Williams, J. Am. Soc. Mass Spectrom. 8 (1997) 565.
[26] T.S. Zwier, J. Phys. Chem. A 105 (2001) 8827.
[27] M. Kohtani, M.F. Jarrold, J. Am. Chem. Soc. 124 (2002) 11148.
[28] K.M. Parkhurst, L.J. Parkhurst, Biochemistry 34 (1995) 293.